

RESEARCH

Open Access



# Function and structure of broadly neutralizing antibodies against SARS-CoV-2 Omicron variants isolated from prototype strain infected convalescents

Dan Li<sup>1†</sup>, Caiqin Hu<sup>2†</sup>, Junwei Su<sup>2†</sup>, Shuo Du<sup>3†</sup>, Ying Zhang<sup>4†</sup>, Wanqi Ni<sup>1</sup>, Li Ren<sup>1</sup>, Yanling Hao<sup>1</sup>, Yi Feng<sup>1</sup>, Changzhong Jin<sup>2</sup>, Shuo Wang<sup>1</sup>, Xinxian Dai<sup>5,6</sup>, Zheng Wang<sup>1\*</sup> , Biao Zhu<sup>2\*</sup>, Junyu Xiao<sup>3,4,7\*</sup> and Yiming Shao<sup>1,2,3\*</sup>

## Abstract

**Background** The ongoing emergence of evolving SARS-CoV-2 variants poses great threaten to the efficacy of authorized monoclonal antibody-based passive immunization or treatments. Developing potent broadly neutralizing antibodies (bNabs) against SARS-CoV-2 and elucidating their potential evolutionary pathways are essential for battling the coronavirus disease 2019 (COVID-19) pandemic.

**Methods** Broadly neutralizing antibodies were isolated using single cell sorting from three COVID-19 convalescents infected with prototype SARS-CoV-2 strain. Their neutralizing activity against diverse SARS-CoV-2 strains were tested in vitro and in vivo, respectively. The structures of antibody-antigen complexes were resolved using crystallization or Cryo-EM method. Antibodyomics analyses were performed using the non-bias deep sequencing results of BCR repertoires.

**Results** We obtained a series of RBD-specific monoclonal antibodies with highly neutralizing potency against a variety of pseudotyped and live SARS-CoV-2 variants, including five global VOCs and some Omicron subtypes such as BA.1, BA.2, BA.4/5, BF.7, and XBB. 2YYQH9 and LQLD6HL antibody cocktail also displayed good therapeutic and prophylactic efficacy in an XBB.1.16 infected hamster animal model. Cryo-EM and crystal structural analyses revealed that broadly neutralizing antibodies directly blocked the binding of ACE2 by almost covering the entire receptor binding motif (RBM) and largely avoided mutated RBD residues in the VOCs, demonstrating their broad and potent neutralizing activity. In addition, antibodyomics assays indicate that the germline frequencies of RBD-specific antibodies

<sup>†</sup>Dan Li, Caiqin Hu, Junwei Su, Shuo Du and Ying Zhang contributed equally to this work.

\*Correspondence:

Zheng Wang  
wangzheng@chinaaids.cn  
Biao Zhu  
zhubiao1207@zju.edu.cn  
Junyu Xiao  
junyuxiao@pku.edu.cn  
Yiming Shao  
yshao@bjmu.edu.cn

Full list of author information is available at the end of the article



increase after an inactivated vaccine immunization. Moreover, the CDR3 frequencies of  $V_{\kappa\lambda}$  presenting high amino acid identity with the broadly neutralizing antibodies were higher than those of  $V_{H}$ .

**Conclusions** These data suggest that current identified broadly neutralizing antibodies could serve as promising drug candidates for COVID-19 and can be used for reverse vaccine design against future pandemics.

**Keywords** SARS-CoV-2, Broad neutralization, Monoclonal antibodies, Hamster model, Cryo-electron microscopy, Antibodyomics assay

## Introduction

SARS-CoV-2 has caused an extremely serious global public health crisis due to its unique pathogenic mechanism and extremely high transmission efficiency. Due to the warned effectiveness of monoclonal antibodies and rapidly evasion from vaccine-induced host immunity, multiple infections of SARS-CoV-2 occurred and could lead to sequelae such as memory loss, weakened immunity, and lung lesions, posing great threat to vulnerable populations [1, 2]. SARS-CoV-2 specific bNabs not only block viral entry of target cells but also kill infected cells through Fc effects such as antibody-dependent cell-mediated cytotoxicity (ADCC) and Antibody-Dependent Cell-Mediated Phagocytosis (ADCP) [3, 4].

Neutralizing antibodies can be administrated early to SARS-CoV-2 infected patients to protect people at high risk of infection. Several neutralizing antibody candidates targeting the SARS-CoV-2 S protein are in clinical trials or are already approved for emergency use, including LYCoV555, REGN-COV2, TY027, CT-P59, JS016, BRII-196, BRII-198, SCTA01, and SA55 [5–7]. However, Omicron sub-variants such as XBB and JN.1 are resistant to most of the antibodies above [8, 9]. Thus, it is urgent to screen more potent, broader and higher production neutralizing antibodies from elite neutralizers of COVID-19 convalescents and explore the potential mechanisms.

SARS-CoV-2 broadly neutralizing antibodies mainly target the N-terminal Domain (NTD) and receptor binding domain (RBD) in S1, and the stem helix (SH) and fusion peptide (FP) in S2 [10]. Among these epitopes, neutralizing antibodies targeting RBD are the most potent. The neutralizing antibodies can be classified into class I, II, III and IV [11]. Class I neutralizing antibodies such as CB6 and CT59 mainly recognize the receptor binding motif (RBM) and the up RBD conformation, which  $V_{Hs}$  originate from IGHV3-53 or IGHV3-66 [12, 13]. Class II RBD antibodies like LY-CoV555 can recognize up or down RBD conformation simultaneously [14]. S309, LY-CoV1404, SP1-77, and REGN10987 classified as class III antibodies bind to the external region of ACE2, as well as up or down RBD [15, 16]. Class IV antibodies such as CR3022, S2X259, ADG20, DH1047, etc. bind to the cryptic region of RBD, but do not directly block the binding of ACE2 to RBD [17]. Despite the progress of the

RBD-specific neutralizing antibodies described above, some questions are still waiting for elucidation. Are there any novel broadly neutralizing antibodies existing in the Chinese elite neutralizers who recovered from prototype SARS-CoV-2 infection? To which classes do these antibodies belong? How about the broadly neutralizing antibody evolution if convalescents received an inactivation vaccine boost?

In this study, we isolated a panel of potent neutralizing antibodies by RBD-specific single B cell sorting from three elite neutralizers selected from 41 COVID-19 convalescents. After evaluating the  $IC_{50}$  values of antibodies against diverse SARS-CoV-2 VOCs, we confirmed that all of them could broadly neutralize all the emerging VOCs and some Omicron variants. We further determined the structures of three antibodies (SWA9, SWC11 and 2YYQH9) in complexes with the spike or RBD that revealed their conserved epitopes within RBD. Moreover, prophylactic and therapeutic administration of an antibody cocktail (2YYQH9 and LQLD6HL) significantly protected golden syrian hamster model against Omicron XBB.1.16 challenge. Also, we resolved the antibodyome at two time points (pre- or post-vaccine immunization) of two convalescents and analyzed the evolutionary pathway of the isolated bNabs. Our results highlight the potential use for antibody-based therapy, prevention and provide a basis for rational vaccine design, which deserves further translational development.

## Materials and methods

### Convalescent patients and blood samples

A total of 41 convalescent patients discharged from the first affiliated hospital, Zhejiang university school of medicine, from February 04 to March 15, 2020, were enrolled in this study (Table S1). The discharge criteria were defined according to “Diagnosis and treatment of novel coronavirus pneumonia”. Whole blood (10 mL) was collected from each donor six months after discharge. Peripheral blood mononuclear cells (PBMCs) were isolated using the Ficoll-Hypaque gradient medium according to the manufacturer’s instruction. Neutralizing activity of plasma against live SARS-CoV-2 was performed. PBMCs were stored at liquid nitrogen for single memory B cell sorting. Donors SW, YYQ and LQL with

broad neutralizing activity against SARS-CoV-2 variants were chosen for antibody isolation. Particularly, donors YYQ and LQL were inoculated with one dose inactivated SARS-CoV-2 vaccine 12 months post-prototype strain infection.

#### Recombinant RBD proteins and probe preparation

Prototype SARS-CoV-2 RBD expression vectors carrying the Avi-tag for biotinylation were constructed. After expression and purification, the proteins were biotinylated by utilizing biotin ligase BirA kit and conjugated with the streptavidin-fluorochrome reagents as previously described [18]. Streptavidin-phycoerythrin (SA-PE) (Sigma) was mixed with biotinylated RBD.

#### Neutralization assay with SARS-CoV-2 pseudovirus

The pseudovirus-based neutralization assay was conducted as described previously [18, 19]. Briefly, 100  $\mu$ L serial dilutions of human plasma or antibodies were added into 96-well plates. After that, 50  $\mu$ L pseudoviruses (1300 TCID<sub>50</sub>/mL) was added into each well, followed by incubation at 37 °C for one hour. Afterward, Vero cells were added into plates ( $2 \times 10^4$  cells/100  $\mu$ L medium per well), followed by incubation at 37 °C and 5% CO<sub>2</sub>. Chemiluminescence detection was performed after 24 hours. The Reed-Muench method was used to calculate the neutralizing activity of plasma or antibody (NT<sub>50</sub> or IC<sub>50</sub>).

#### Isolation of RBD-specific memory B cells by single cell sorting

PBMCs were incubated with an antibody cocktail including: anti-CD3-Pacific Blue, anti-CD8-Pacific Blue, anti-CD19-BV570, anti-CD27-APCCy7, anti-IgG-FITC, anti-IgM-PercpCy5.5, anti-CD4-BV605 (all from BD Biosciences), anti-CD20-ECD (Becman Coulter), anti-CD14-eluor450 (ebioscience), and anti-RBD-PE. Dead cells were excluded using the Live/Dead Fixable dead cell stain kit (355 nm excited, Invitrogen). Thereafter, cryopreserved PBMC were thawed, washed and surface stained with the above antibody cocktail and prototype RBD probe in a total volume of 50  $\mu$ L on ice in dark for one hour, followed by Live/Dead staining. The stained PBMC were filtered by 70- $\mu$ m cell mesh (BD Biosciences) and sorted using a five-laser FACSARIA SORP. CD3<sup>-</sup>, CD8<sup>-</sup>, DAPI<sup>-</sup>, CD14<sup>-</sup> CD19<sup>+</sup>, CD20<sup>+</sup>, CD27<sup>+</sup>, IgM<sup>-</sup>, IgG<sup>+</sup>, RBD<sup>+</sup> cells were defined as SARS-CoV-2 specific memory B cells and were sorted into 96-well PCR plates containing 20  $\mu$ L of cell lysis buffer per well under single mode. The PCR plates with sorted cells were quickly frozen on dry-ice and stored at -80 °C overnight. RT-PCR were performed to amplify the variable regions of heavy chain and light chain as previously reported [20].

#### Antibody expression and purification

The V<sub>H</sub> and V<sub>K</sub>/V <sub>$\lambda$</sub>  genes were cloned into the CMV/R expression vector containing the constant regions of IgG1 heavy chain or light chain. Paired IgG heavy chain and light chain plasmids were co-transfected into 293F cells, then cells were incubated at 37 °C in a humidified 8% CO<sub>2</sub> environment for five days. Supernatants were collected and antibodies were purified using protein A column (Pierce). The antibody concentration was determined by Nanodrop 2000 ultramicro spectrophotometer (Thermo) and stored at 4 °C for detection.

#### Measurement of antibody binding kinetics with SARS-CoV-2 RBD

Antibody-antigen kinetics (K<sub>D</sub>) between antibodies and SARS-CoV-2 prototype RBD was measured by a Biacore T200 (Cytivia, USA) with anti-His sensor chip CM5 (Cat no.BR100530, Cytiva, USA) at room temperature. In brief, SARS-CoV-2 RBD-His tag protein was immobilized on the chip in sodium acetate buffer (pH 5.0) for a final response unit. Gradient concentrations of five antibodies (50 nM, 25 nM, 12.5 nM, 6.25 nM, 3.125 nM and 1.5625 nM) were then flowed onto the chip surface in the running buffer containing 0.01 M HEPES, 0.15 M NaCl, 0.003 M EDTA and 0.05% Tween-20. The sensor was regenerated with acid glycine (PH 1.5) after each cycle. Affinity (K<sub>a</sub>, K<sub>d</sub> and K<sub>D</sub>) was calculated using a 1:1 binding model with a Biacore T200 evaluation software (version 3.2).

Kinetics between antibodies and Omicron variant RBD was evaluated using an Octet RED96 instrument. Briefly, biotinylated RBD of Omicron variant at 1  $\mu$ g/mL in kinetic buffer (0.02% Tween-20 and 0.1% Albumin bovine serum in PBS) was immobilized on the surface of SA capture biosensors (185,045, ForteBio, USA) for 60 s. After that, the biosensors were immersed into twofold serial dilutions of mAbs for 120 s and then to buffer for 300 s to acquire association and dissociation constants separately. The data was processed by Data Analysis HT 9.0 software. K<sub>D</sub>, K<sub>on</sub> and K<sub>off</sub> values were calculated using a 1:1 binding model by a global fitting method.

#### Neutralizing activity of mAbs against authentic SARS-CoV-2

Authentic SARS-CoV-2 viruses were propagated in Vero-E6 cells. To analyze the mAb's neutralizing activity, two-fold serial dilutions of mAbs were added into 100 TCID<sub>50</sub> of SARS-CoV-2, followed by one hour incubation at 37 °C. The mixture was added to a monolayer of Vero-E6 cells in a 96-well plate and incubated at 37 °C. Cytopathic effects (CPE) were observed and

recorded from day 4 to day 6. The antibody concentration at which cytopathic effect presented in half wells was defined as  $IC_{50}$ .

#### Protein expression and purification for cryo-EM study

The S6P (B.1.617.2) expression construct that encodes the spike ectodomain (residues 1–1208) with six stabilizing Pro substitutions (F817P, A892P, A899P, A942P, K986P, and V987P) and a “GSAS” substitution at the furin cleavage site (residues 682–685) was previously described [21]. Additional mutations (T19R, G142D,  $\Delta$ 156–157, R158G, L452R, T478K, D614G, P681R, D950N) were introduced into this construct using site-directed mutagenesis to generate the S6P (B.1.617.2) expression vector. The S6P (B.1.617.2) protein, as well as the antigen-binding fragments (Fabs) of SWA9 and SWC11, was transiently expressed in the HEK293F cells and purified using the Ni–NTA affinity and size-exclusion chromatographies. The final protein storage buffer is 20 mM HEPES, pH 7.2, and 150 mM NaCl.

#### Cryo-EM data collection, processing, and structure building

To prepare the sample for cryo-EM study, four microliter S6P (B.1.617.2) protein (0.9 mg/mL) was mixed with the same volume of SWA9 or SWC11 Fab (1 mg/mL), and immediately applied onto the glow-discharged holy-carbon gold grids (Quantifoil, R1.2/1.3) in an FEI Vitrobot IV (4 °C, 100% humidity). The grids were then flash cooled in liquid ethane and screened using a 200 kV Talos Arctica electron microscope. Good grids were transferred to a 300 kV Titan Krios G3i electron microscope for data collection using a K3 direct detection camera. A total of 2932 and 2726 movies were recorded for the S6P (B.1.617.2)/SWA9 and S6P (B.1.617.2)/SWC11 samples, respectively. Cryo-EM data were processed using the cryoSPARC software [22] following a procedure we established previously [23]. Structure modeling and refinement were performed using Coot and Phenix [24]. Figures were prepared using UCSF ChimeraX [25]. Cryo-EM data collection, processing and validation statistics were shown in Table S2.

#### Crystallization, data collection and structure determination of 2YYQH9-RBD complex

The RBD/2YYQH9-Fab complex was concentrated to 10 mg/mL for crystallization. Crystals were grown at 20 °C using the sitting-drop vapor diffusion method. The crystallization solution contains 13% (w/v) PEG 10000, 100 mM Sodium citrate/ Citric acid pH 5.75, 2% (v/v) Dioxane. For data collection, the crystals were transferred to a solution containing the crystallization solution supplemented with 5% ethylene glycol and

flash-cooled in liquid nitrogen. Diffraction data were collected at the Shanghai Synchrotron Radiation Facility (beamline BL10U2) and processed then using HKL2000 (HKL Research). The structures were solved by molecular replacement using PHASER, adjusted in COOT and refined using PHENIX.

#### In vivo efficacy in a hamster model

Four groups of female golden syrian hamster ( $n=6$  per group) from six- to eight-week-old were housed in an ABSL-3 lab under the National Vaccine & Serum institute (NVSI) guidelines. All animals were inoculated with 100  $\mu$ L of SARS-CoV-2 XBB.1.16 solution ( $10^{6.125}$  TCID<sub>50</sub>/mL) via intranasal drips. For the prophylactic experiments, four hours prior to SARS-CoV-2 infection, hamsters in group A and group B received 20 mg/kg antibody cocktail i.p. (intraperitoneal) or i.n. (intranasal) in a volume of 100  $\mu$ L, respectively. For the therapeutic strategy, 24 hours after SARS-CoV-2 infection, hamsters were administered 100  $\mu$ L of a 20 mg/kg dose of the above mAbs i.p. The animals in the control group were administered anti-HIV human mAb at an equivalent volume. Viral load of nasal swabs were measured before infection and seven days post-infection. Five hamsters per group were euthanized at the seventh day post-infection and the viral loads in lung, trachea, turbinalia and intestine tissues were examined. Histopathological changes in lungs were identified by Hematoxylin and Eosin (H&E) stain after fixed in 4% paraformaldehyde solution.

#### Unbiased antibodyomics analysis of donor SW and YYQ

Total RNA was extracted from donors' PBMCs using an RNeasy mini kit (Cat.74104, Qiagen, Germany). Then, unbiased antibody library containing  $V_H$ ,  $V_K$  and  $V_\lambda$  were prepared using a SMARTer Race 5'/3' Kit (Cat.634858, Takara, Japan) as previously described [18]. After deep sequencing by Illumina Miseq PE300, the cleaned sequencing data were initially evaluated using IMG/HighV-QUEST online tool (<http://imgt.org/HighV-QUEST/index.action>), and further analyzed with related R package.

#### Statistical analysis

Statistical analyses were performed using R-4.3.2 software. The comparisons between groups were performed using the Wilcoxon test. \*,  $p<0.05$ ; \*\*,  $p<0.01$ ; and \*\*\*,  $p<0.001$  were considered statistically significant.

## Results

#### Isolation of RBD-specific antibodies of three elite neutralizers screened from 41 COVID-19 convalescents

Forty-one COVID-19 convalescents were enrolled in the study, who were discharged from the first

affiliated hospital, Zhejiang University School of Medicine, between February 04 and March 15 in 2020 (Table S1). Peripheral blood samples were collected at 6 months after discharge. The neutralizing activity of plasma was analyzed by authentic viruses neutralization assay using prototype, B.1.351, P.1 and B.1.617.2, respectively. From them, we chose three patients (SW, YYQ and LQL) with broadly neutralizing activity against SARS-CoV-2 variants for antibody isolation.

To isolate RBD-specific memory B cells, we stained  $1 \times 10^7$  peripheral blood mononuclear cells (PBMCs) from each donor by cocktail antibodies plus phycoerythrin (PE)-labeled RBD probe and sorted them by a FACS Aria Cell Sorter III machine (Fig. 1a). We isolated 56, 114 and 46 single B cells from SW, YYQ and LQL, respectively, and then subjected them to  $V_H/V_L$ -specific PCR amplification. Briefly, 32, 87 and 28 paired  $V_H$  and  $V_L$  genes from convalescents SW, YYQ and LQL were acquired, sequenced, and analyzed sequentially. For donor SW,  $V_H$  genes originated from IGHV1, IGHV3, IGHV4, IGHV5 and IGHV7 germ lines, and IGHV3 and IGHV4 presented 34.34% (11/32) and 37.5% (12/32) respectively (Fig. 1b). For  $V_{\kappa/\lambda}$  genes, IGKV1 accounted for 50% (10/20) in the  $\kappa$  chain and IGLV2 made up 58.3% (7/12) in the  $\lambda$  chain. Similar results were observed in the donor YYQ and LQL. IGHV3 presented 58.6% (51/87) and 53.6% (15/28) in YYQ and LQL respectively, and IGKV1 accounted for 75.7% (53/70) in  $\kappa$  chains of YYQ and 68.7% (11/16) in  $\lambda$  chains of LQL respectively (Fig. 1b).

Somatic hypermutation (SHM) rates and length of the third complementarity determining region (CDR3) of the heavy chain immunoglobulin (Ig) are key parameters to evaluate the maturation level of antibodies. The average SHM rates of  $V_H/V_{\kappa/\lambda}$  were around 7% and 4%, respectively, and the median CDR3 lengths of  $V_H/V_{\kappa/\lambda}$  were 14 amino acids (AA) and 9 AA, respectively (Fig. 1c). YYQ and LQL also presented similar sequence characteristics to SW (Fig. 1c). Next, we digested PCR products of  $V_H/V_{\kappa/\lambda}$  by restriction enzymes and ligated them to the corresponding IgG expression vectors. After expression and purification, we produced 24, 44 and 28 RBD-specific antibodies from SW, YYQ and LQL respectively and evaluated their neutralizing activity using a SARS-CoV-2 prototype pseudovirus (Fig. S1).

#### Neutralizing activity of antibodies against SARS-CoV-2 pseudoviruses and live SARS-CoV-2 viruses

We selected six antibodies (SWA9, SWB8 and SWC11 from SW, 2YYQH9 and 2YYQF10 from YYQ, and LQLD6HL from LQL) whose  $IC_{50}$  values against prototype virus were less than 0.1  $\mu\text{g}/\text{mL}$  for further neutralization testing. We then tested the neutralizing activity

of antibodies versus VOCs, e.g., B.1.1.529, BA.2, BA.4, BF.7 and XBB (Fig. 2a, b). For the neutralizing activity against pseudoviruses, five antibodies (SWA9, SWB8, SWC11, 2YYQH9 and LQLD6HL) neutralized prototype, B.1.1.529, BA.2 and BF.7 pseudoviruses (Fig. 2a). Notably, XBB escaped SWA9, SWB8 and SWC11; however 2YYQH9 and LQLD6HL efficiently neutralized all variants with potency less than 1  $\mu\text{g}/\text{mL}$ , indicating their powerful neutralizing activity against VOCs (Fig. 2a). Importantly, LQLD6HL potently inhibited the XBB variant with  $IC_{50}$  values of 0.045  $\mu\text{g}/\text{mL}$ .

We nextly measured the neutralizing activity of five antibodies (SWA9, SWB8, SWC11, 2YYQH9 and 2YYQF10) against live viruses including prototype, P.1, B.1.351, B.1.617.2, B.1.1.529, BA.1, BA.2 and BA.5 variants using a viral cytopathic effect (CPE)-based method on Vero cells. As Fig. 2b shows, these five antibodies nearly neutralized all the VOCs with  $IC_{50}$  values below 5  $\mu\text{g}/\text{mL}$  except for SWA9, which could not inhibit BA.5. Particularly, SWB8 and 2YYQH9 efficiently inhibited all the variants with  $IC_{50}$  values less than or slightly over 1  $\mu\text{g}/\text{mL}$ . This observation suggests that SWB8 and 2YYQH9 have potential against the VOCs.

#### Binding kinetics of antibodies with SARS-CoV-2 prototype and Omicron RBD

Binding kinetics between antibodies and prototype RBD were evaluated using a Surface Plasmon Resonance (SPR) method or a bio-layer interferometry (BLI) method. As depicted in Fig. S2a, antibodies bind RBD with  $K_D$  values as follows: SWA9 (0.345 nM), SWB8 (0.325 nM), SWC11 (0.627 nM), 2YYQH9 (0.428 nM), 2YYQF10 (<0.001 nM) and LQLD6HL (0.33 nM). Compared to other broadly neutralizing antibodies such as P2C-1F11 (2.12 nM), P2B-2F6 (5.14 nM) [26], CB6 (2.49 nM) [12] and BD368 (1.2 nM) [27], the lower  $K_D$  values of these six antibodies suggest that they have greater affinity with prototype RBD and may be related with higher neutralizing activity against prototype virus.

Next, binding kinetics between the antibodies and Omicron RBD (B.1.1.529) was tested with the BLI method. As shown in Fig S2.b,  $K_D$  values were as follows: SWA9 (<0.001 nM), SWB8 (<0.001 nM), SWC11 (<0.001 nM), 2YYQH9 (<0.001 nM), 2YYQF10 (0.874 nM) and LQLD6HL (2.35 nM). In comparison with  $K_D$  values with prototype RBD, the SWA9, SWB8, SWC11 and 2YYQH9 antibodies presented much lower  $K_D$  values with B.1.1.529 RBD while 2YYQF10 and LQLD6HL showed higher  $K_D$  values with B.1.1.529 RBD. These results indicate that SWA9, SWB8, SWC11 and 2YYQH9 have comparably powerful neutralizing activity against B.1.1.529 as well as prototype virus, which is in accordance with the data shown in Fig. 2a.

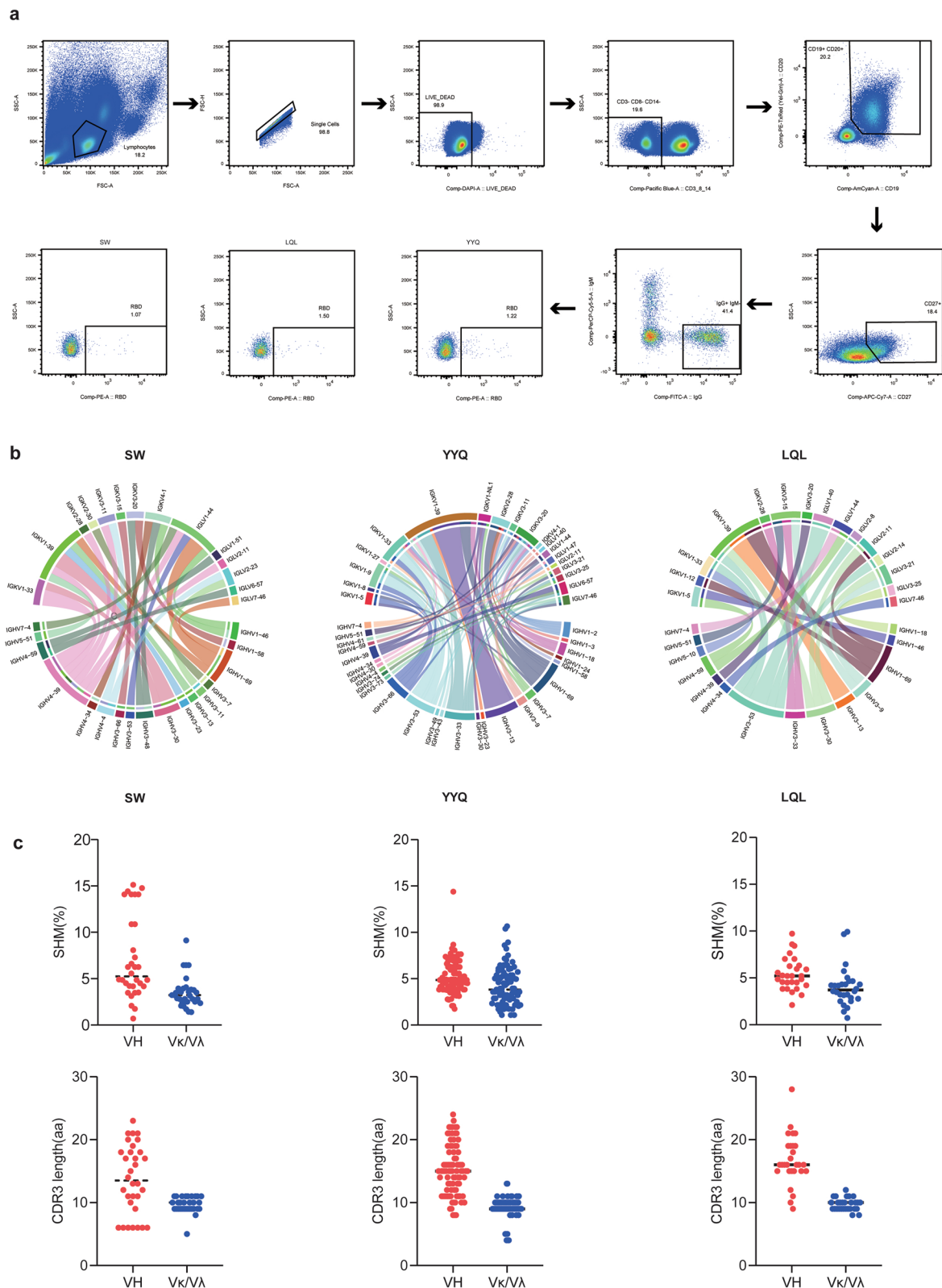


**Fig. 1** Isolation of RBD-directed memory B cells by cell sorting. **(a)** PBMCs gated on total live CD3<sup>+</sup>CD8<sup>-</sup>CD14<sup>-</sup>CD19<sup>+</sup>CD20<sup>+</sup>CD27<sup>+</sup>IgG<sup>+</sup>RBD<sup>+</sup>B cells were sorted from convalescent patients YYQ, SW and LQL, respectively. **(b)** Chord diagram representation of V and J frequency of isolated antibodies from YYQ, SW and LQL, respectively. The size of the inner segments corresponds to the number of sequences of each gene, and the color-coded diagrams indicate the pairing network of the V<sub>H</sub> and V<sub>J</sub>. **(c)** SHM rates and CDR3 lengths of V<sub>H</sub> and V<sub>κ/Vλ</sub> of SW, YYQ and LQL, respectively

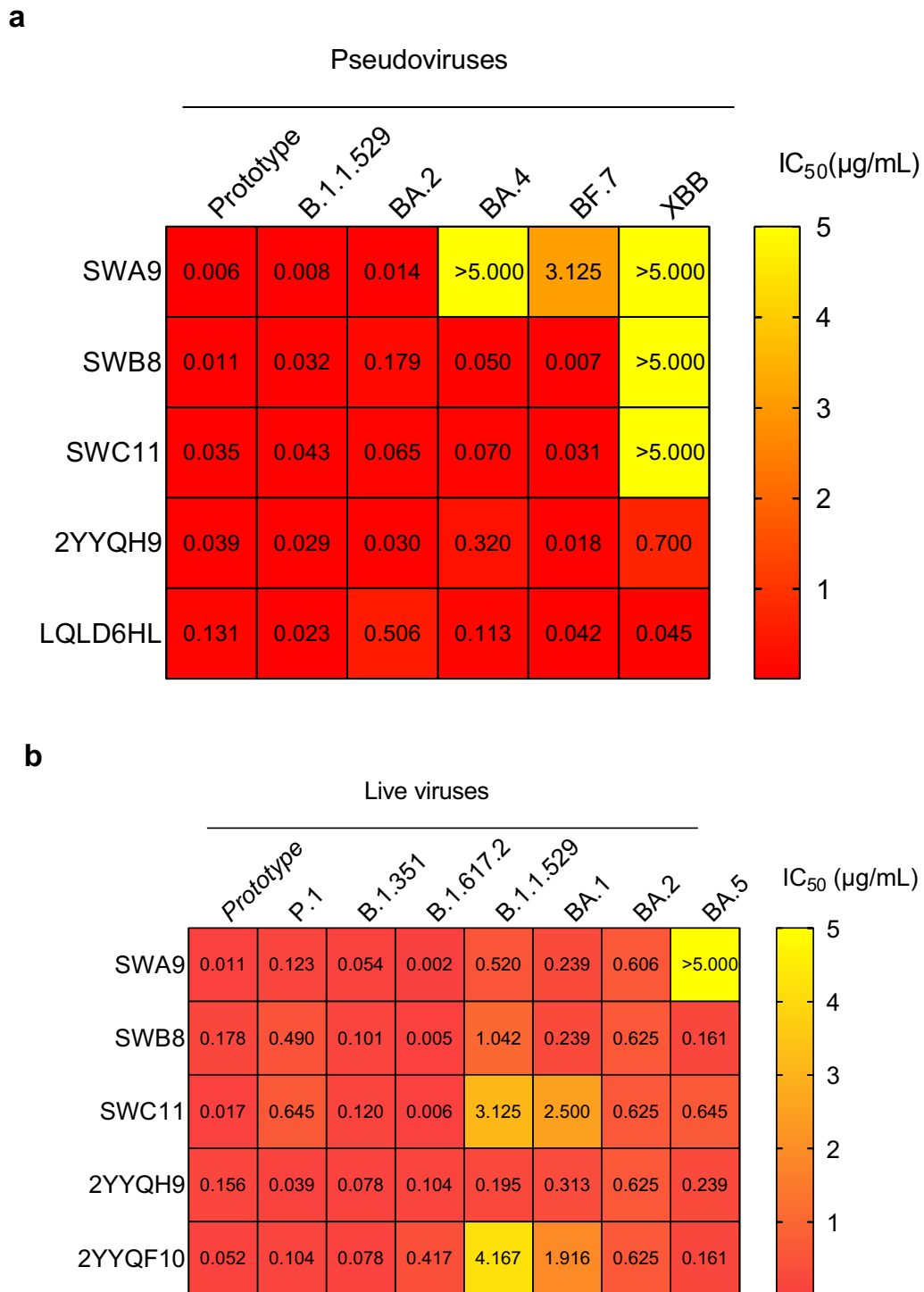


**Fig. 2** Heatmap of neutralizing activity (IC<sub>50</sub>, μg/mL) of antibodies against multiple SARS-CoV-2 variants. **(a)** pseudoviruses, **(b)** live viruses

Taken together, antibodies SWA9, SWC11 and 2YYQH9 had broader neutralizing activity, higher binding affinity with Omicron RBD and superior expression efficiency among the tested antibodies, thus these three

antibodies were selected to resolve antigen–antibody complex structures. Particularly, SWA9 and SWC11 were isolated during the B.1.617.2 outbreak, and 2YYQH9 was isolated later.

### Cryo-EM structure of SWA9 bound to S6P (B.1.617.2)

SWA9 was selected for structural analysis for its higher neutralization potency. To understand the neutralization mechanism of SWA9, we used cryo-electron microscopy (cryo-EM) to determine the structure of the SWA9 Fab bound to a prefusion-stabilized B.1.617.2 spike trimer, S6P (B.1.617.2), at 3.2 Å. In the presence of the SWA9 Fab, the S6P (B.1.617.2) trimer adopted an open conformation with all three RBDs in ‘up’ positions, each was occupied by a SWA9 Fab (Fig. 3a). SWA9 binds to the left shoulder of RBD [28], which is reminiscent of BD-368, a super potent neutralizing antibody that we characterized previously [27]. All three heavy-chain complementary-determining regions (HCDR1-3) and two Kappa-chain CDRs (KCDR1, KCDR3) of SWA9 are involved in interacting with RBD, burying a surface area of  $\sim 725$  Å<sup>2</sup>. The heavy chain of SWA9 would directly compete with ACE2 (Fig. 3a). The epitope of SWA9 consists of several hydrophobic RBD residues, including Leu455, Phe456, Phe486, and Tyr489. Furthermore, RBD residues such as Ala475, Ser477, Pro479, Asn487, and Gln493 are likely probed by SWA9 via hydrogen bond interactions.

The recently emerging B.1.1.529 variant has raised concerns worldwide due to the large number of mutations it carries. In particular, 15 of these mutations are found in the RBD, including G339D, S371L, S373P, S375F, K417N, N440K, G446S, S477N, T478K, E484A, Q493R, G496S, Q498R, N501Y, and Y505H, leading to the escape of B.1.1.529 from a large number of neutralizing antibodies [29]. Importantly, SWA9 potentially neutralized the B.1.1.529 pseudovirus and the live virus (Fig. 2b). Thus, the structure of SWA9 in complex with the B.1.617.2 spike can be used to rationalize its exceptional potency. Among the 15 mutated sites in the B.1.1.529 RBD,

Ser477, Thr478, and Gln493 are within the epitope of SWA9. Ser477 forms a hydrogen bond interaction with SWA9 via its main chain amide group (Fig. 3a), which is not sensitive to the side chain substitution. The T478K mutation is present in the B.1.617.2 spike and is captured in our structure. The Lys may form hydrogen bonds with several light chain residues in SWA9, leading to a more favorable interaction between SWA9 and RBD. Gln493, which is in the periphery of the SWA9 epitope, only has a marginable interaction with SWA9 (Fig. 3a). Consistently, the Q493R mutation does not affect the neutralizing activity of SWA9 towards B.1.1.529.

### Cryo-EM structure of SWC11 bound to S6P (B.1.617.2)

SWC11 was chosen for structure analysis because it belongs to the VH3-53 germline, a typical class I (group A) antibody. We also determined a 3.0 Å cryo-EM structure of S6P (B.1.617.2) in complex with the Fab of SWC11. In this structure, the S6P (B.1.617.2) trimer also displayed a fully open conformation, and all three ‘up’ RBDs were engaged with SWC11 (Fig. 3b). SWC11 is a VH3-53 germline gene-encoded antibody and interacts with the RBD via a typical class I VH3-53/VH3-66 antibody binding mode. Like other antibodies in this class, the epitope of SWC11 largely overlaps with the binding site of ACE2, involving RBD residues Arg403, Lys417, Tyr421, Tyr453, Leu455, Phe456, Tyr473, Gln474, Ala475, Ser477, Phe486, Asn487, Tyr489, and Tyr505. In B.1.351 and P.1, the positively charged Lys417 is mutated to the neutral residues Asn and Thr, respectively. Compared to B.1.617.2, B.1.351 and P.1 both contain the mutations Glu484Lys, and Asn501Tyr, while B.1.1.7 also contains the Asn501Tyr mutation. B.1.617.2 contains the mutations leu452Arg and Thr478Lys, which are not

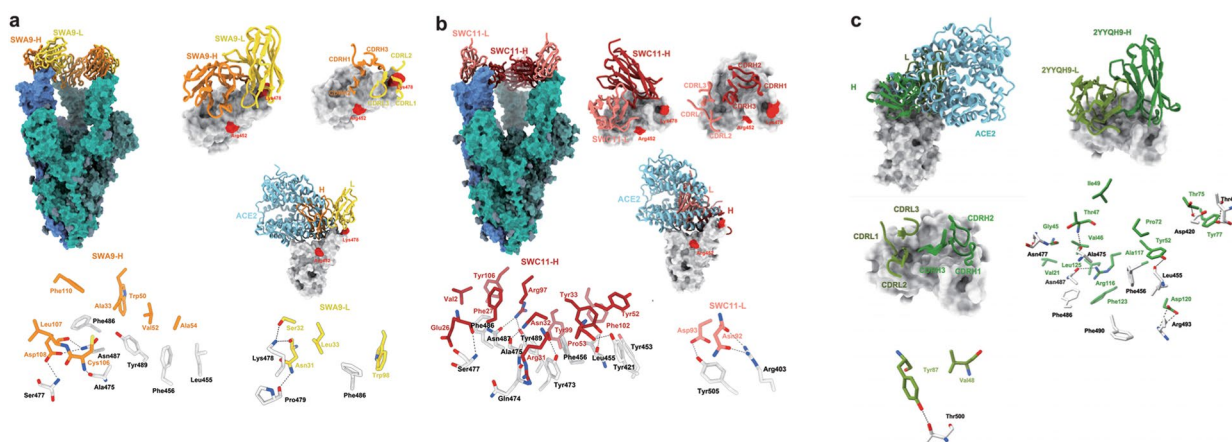


**Fig. 3** Structure of antibody–antigen complexes of SWA9, SWC11 and 2YYQH9. **(a)** Structure of the prefusion S6P (B.1.617.2) trimer with three SWA9 Fabs bound to three ‘up’ RBDs. **(b)** Structure of the prefusion S6P (B.1.617.2) trimer with three SWC11 Fabs bound to three ‘up’ RBDs. **(c)** Crystallization and structure of stable 2YYQH9 and RBD (BA.1.1.529.1) complex

present in B.1.1.7, B.1.351, and P.1. Importantly, Lys417 only weakly interacts with SWC11, whereas Glu484 and Asn501 are not part of SWC11's epitope. SWC11 also does not contact Arg452 in the B.1.617.2 spike and may contact Lys478 via an acidic residue (Fig. 3b). Thus, SWC11 remains potent towards B.1.1.7, B.1.351, P.1, B.1.617.1 and B.1.617.2 that have mutations in these positions. As for RBD residues that are mutated in B.1.1.529, and Lys417, Ser477, Gln493 and Tyr505 are also targeted by SWC11 (Fig. 3b). However, it appears that none of these residues make critical interactions with SWC11. The neutralization results against pseudoviruses suggest that the combined mutations of these residues only slightly diminished the neutralizing activity of SWC11.

#### Structure of 2YYQH9 Fab and RBD (BA.1.1.529.1) complex and their interactions

2YYQH9 is encoded by the VH3-53 gene and is classified as class I neutralizing antibodies which epitopes extensively coincide with the ACE2 binding interface. These antibodies predominantly consist of VH3-53/VH3-66 germline gene-encoded antibodies and are prominently featured in our current collection of SARS-CoV-2 neutralizing antibodies. 2YYQH9 was chosen for structure comparison with SWC11 since it also belongs to VH3-53. To delve into the structural underpinnings of the 2YYQH9 Fab binding to the RBD, the crystal structure of the 2YYQH9 Fab and the RBD (BA.1.1.529.1) complex was resolved at a high resolution of 2.73 Å. In alignment with other class I neutralizing antibodies, the epitope of 2YYQH9 overlaps with the ACE2-binding motif (Fig. 3c). The comprehensive structure elucidates that 2YYQH9 interacts with the RBD, covering a buried surface area of 1136 Å<sup>2</sup>, with the V<sub>H</sub> and V<sub>L</sub> domains occupying 791 Å<sup>2</sup> and 345 Å<sup>2</sup>, respectively. The epitope of 2YYQH9 is primarily composed of RBD residues including Arg403, Asp405, Arg408, Thr415, Gly416, Asn417, Asp420, Tyr421, Tyr453, Leu455, Phe456, Arg457, Lys458, Ser459, Asn460, Tyr473, Asn474, Ala475, Gly476, Asn477, Phe486, Asn487, Tyr489, Phe490, Arg493, Tyr495, Ser496, Arg498, Thr500, Tyr501, Gly502, and His505 (Fig. 3c). Notably, residues such as Phe456, Phe486, and Phe490 engage in hydrophobic and van der Waals interactions with 2YYQH9, while residues like Thr415, Asp420, Leu455, Ala475, Asn477, Asn487, Arg493, and Thr500 are involved in polar interactions (Fig. 3c).

Within the RBD of the B.1.1.529.1 variant, there are 15 mutated sites, among which Ser477 and Gln493 are located within the epitope recognized by the antibody 2YYQH9. Ser477 establishes a hydrogen bond with 2YYQH9 through its main chain amide group, a bond that remains unaffected by side chain substitutions. Additionally, the Q493R mutation, which is present in

the B.1.1.529 variant, is incorporated into our structural analysis. This mutation has the potential to form a hydrogen bond with residues in the high chain of 2YYQH9, thereby enhancing the affinity between 2YYQH9 and the RBD.

SWC11 and 2YYQH9, both from the VH3-53 germline, primarily rely on the heavy chain and share epitope residues at positions 417, 421, 455, 456, 475, 486, 487, and 489. Although SWA9 does not belong to VH3-53, its epitope overlaps significantly with those of VH3-53 antibodies, including residues 455, 456, 486, 487, and 489, which are also part of the ACE2 binding site. In summary, the epitopes of these three antibodies show high overlap with the ACE2 binding site, particularly for 2YYQH9, which may explain why 2YYQH9 is difficult for the virus to evade.

#### In vivo efficacy of the 2YYQH9 and LQLD6HL combination in the SARS-CoV-2 infected golden Syrian hamster model

To evaluate the efficiency of 2YYQH9 and LQLD6HL antibodies in protecting hamsters from SARS-CoV-2 XBB.1.16 infection, we initially assessed the impact of the two mAbs in both prophylactic and treatment settings. Hamsters in prophylactic groups (group A and group B) received antibody cocktail (2YYQH9 and LQLD6HL) i.p. or i.n. four hours prior to SARS-CoV-2 infection, respectively. The same mAbs were administered i.p. 24 hours after virus challenge in group C. Group D administered i.p. with anti-HIV human mAb 24 hours post-challenge was set as the control group (Fig. 4a). We sacrificed one mouse per group at day 5 to check the pathology of lungs and other tissues, and all the other mice were alive at day 7 until the end of the study (Fig. S4). Although significant changes in body weight between four groups were not observed, the SARS-CoV-2 viral load in tissues including lung trachea and intestine in group A and B were decreased when compared to the control group (Fig. S4 and Fig. 4c). Additionally, viral load in the nasal swabs in group A were reduced during the daily monitor period, especially in day 3 and day 5 (Fig. 4b). Furthermore, the pathology analyses showed evidence of mild pneumonia in the control group, which was characterized by inflammatory cell infiltration, alveolar septal thickening, and distinctive vascular system injury. In contrast, prophylactically and therapeutically treated animals showed limited pathological features in lung when compared with the control group (Fig. 4d).

#### Antibody repertoires of donors SW and YYQ during vaccine immunization

The antibody repertoires of donors SW and YYQ were evaluated in two time points (pre- and post- vaccination). The V<sub>H</sub>, V<sub>K</sub> and V<sub>L</sub> of two time points (pre- and

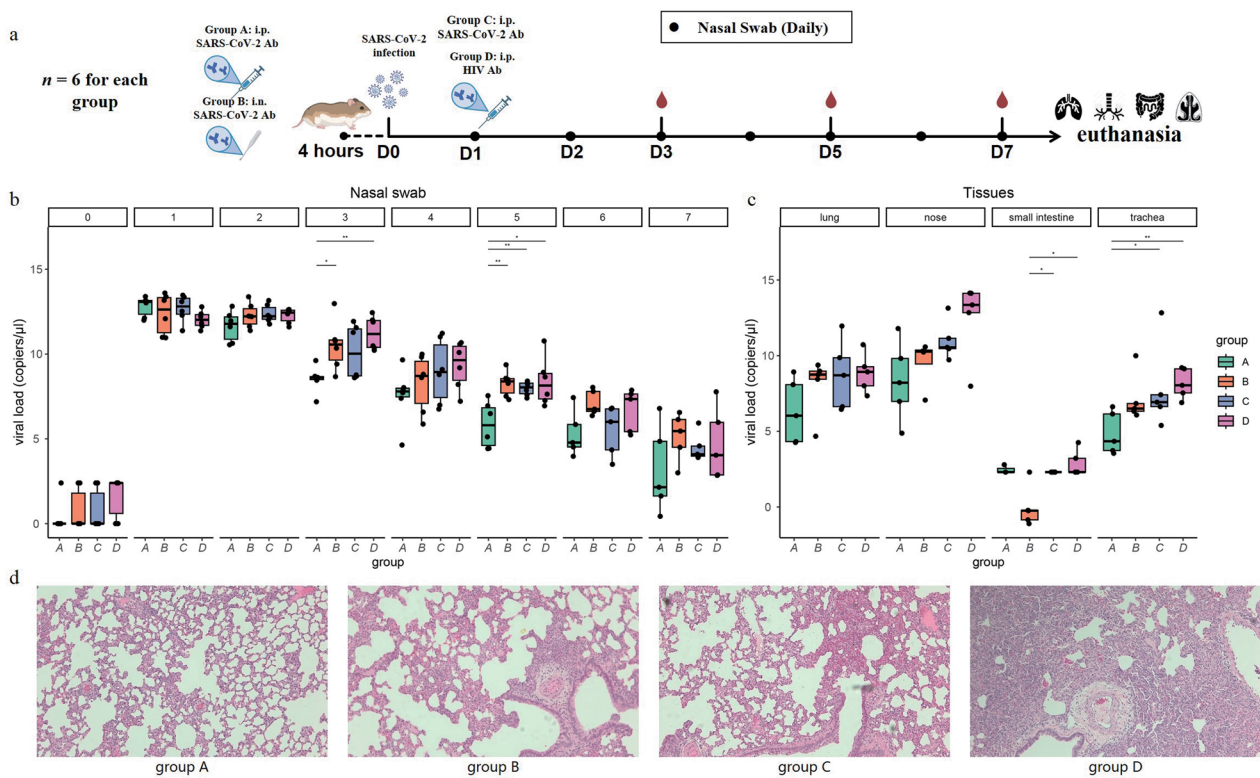


**Fig. 4** The effective protection of antibody cocktails in golden Syrian hamsters challenged with SARS-CoV-2 XBB.1.16. **(a)** Groups of hamsters that infected SARS-CoV-2 were divided into four groups ( $n=6$  per group). All animals were challenged with SARS-CoV-2 XBB.1.16 intranasally and 20 mg/kg antibodies were administered i.p (group A) or i.n (group B) four hours prior-infection, and i.p (group C) 20 hours post-infection. Equal volume of anti-HIV antibody was used as a control (group D). **(b)** Viral load of nasal swabs were monitored daily. **(c)** Viral load in lung, trachea, turbinalia and intestine tissues were examined at day 7. **(d)** Representative histopathology of lungs in hamsters of four groups. The images are shown as 100 $\times$

post- vaccination) of the donors SW and YYQ were unbiasedly amplified using the 5'-RACE PCR method and deeply sequenced using Illumina Miseq V3 machine. For donor SW, in brief, 622,607  $V_H$  sequences, 411,747  $V_K$  sequences and 816,507  $V_L$  sequences covering full-length variable regions (>300 bp) were acquired in the first time point, and 1,023,403  $V_H$  sequences, 778,796  $V_K$  sequences and 527,845  $V_L$  sequences containing full-length variable regions were obtained in the second time point. For donor YYQ, in the first time point, 232,543  $V_H$  sequences, 485,295  $V_K$  sequences, and 328,677  $V_L$  sequences containing full-length variable regions were acquired. Similarly, in the second time point, 222,782  $V_H$  sequences, 464,755  $V_K$  sequences, and 320,509  $V_L$  sequences containing full-length variable regions were obtained.

Some germline frequencies of  $V_H$ ,  $V_K$  and  $V_L$  were greatly changed after vaccination for donor SW (Fig. 5a). In the first time point, IGHV4-59 (8.0%), IGKV4-1 (13.1%) and IGLV2-14 (22.3%) accounted for the highest percentages in  $V_H$ ,  $V_K$  and  $V_L$ , respectively. In contrast,

IGHV3-7 (9.60%), IGKV4-1 (20.2%) and IGLV2-14 (17.6%) presented the highest frequency in the repertoire at the second time point.

A few germline frequencies were increased substantially in the second time point after vaccination. Particularly, all the  $V_H$  and  $V_{K/L}$  germline frequencies of the broadly neutralizing antibodies SWA9 (0.03% vs. 0.13% for IGHV1-58 and 7.31% vs. 8.50% for IGKV3-20), SWB8 (0.94% vs. 3.37% for IGHV3-48 and 13.11% vs. 20.20% for IGKV4-1) and SWC11 (0.85% vs. 1.09% for IGHV3-53 and 0.82% vs. 1.25% for IGKV3D-15) increased after vaccination in donor SW. These results indicate that these germlines are activated by the vaccine inoculation (Fig. 5a).

A crucial factor for the evolutionary level of SARS-CoV-2 Nabs is the SHM rate. Most RBD-specific neutralizing antibodies present SHM rates less than 10%. In this study, it was discovered that  $V_H$  SHM rates clustered between 3% and 11%. The percent repertoire of SHM below 5% and over 10% both rose significantly for  $V_H$ , while SHM over 5% and 6% increased for  $V_K$  and

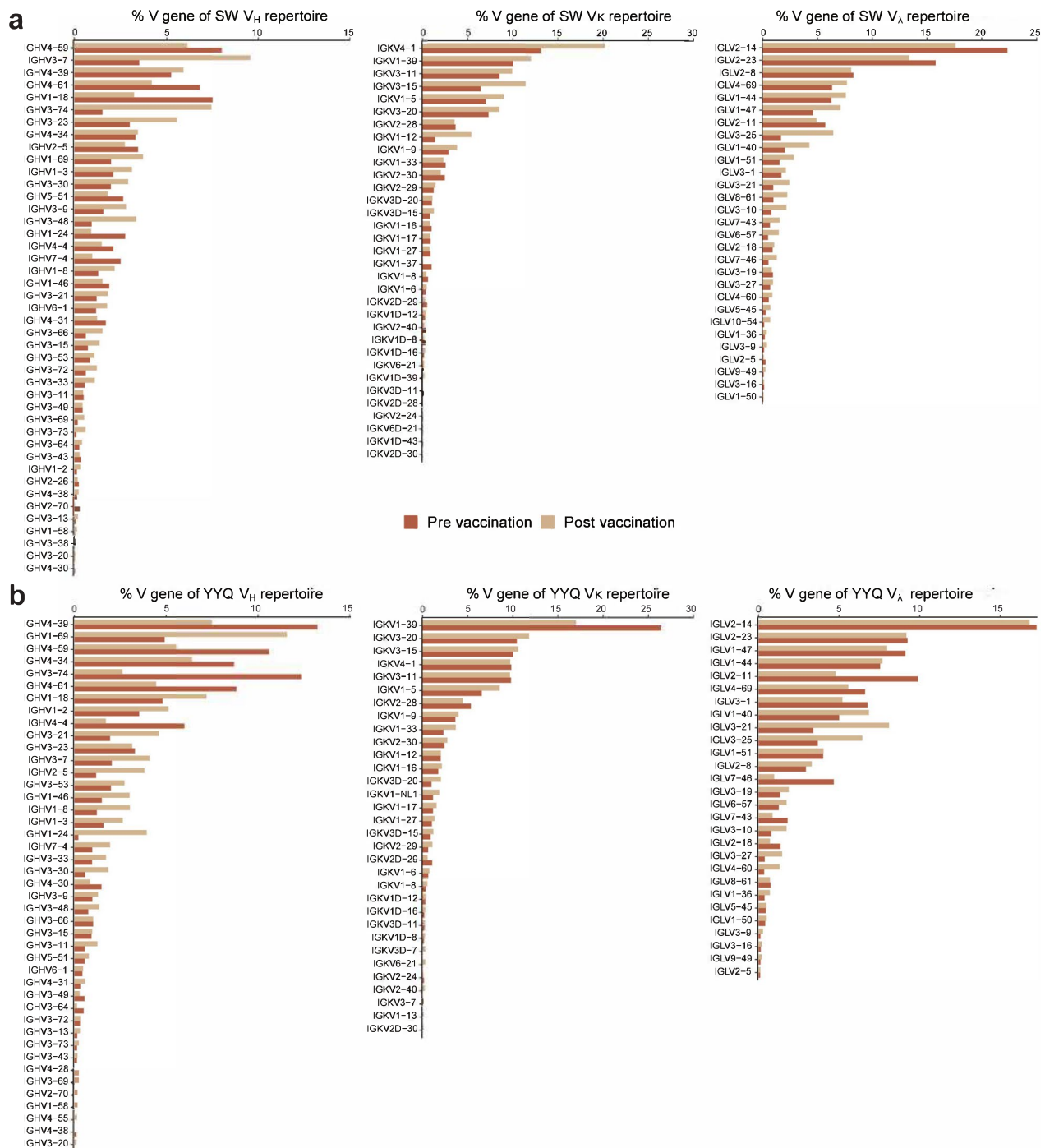


**Fig. 5** Germline distributions of variable regions of heavy chains and light chains of donors from two timepoints (pre- and post- immunization). (a) Donor SW. (b) Donor YYQ

$V_{\lambda}$  respectively, after vaccine immunization (Fig. S3a). Another key factor in determining the evolutionary stage of SARS-CoV-2 Nabs is the HCDR3 length. Most of the HCDR3 lengths of RBD-specific neutralizing antibodies in our research were between 10 and 13 AA.

HCDR3 length varied from 5 to 25 AA, and the proportion of sequences with 10 to 15 AA HCDR3 increased after vaccination. In terms of lambda chain, the majority of LCDR3 lengths ranged from 9 to 15 AA, and following vaccination, the percent repertoire of sequences with

8 AA, 11 AA, and 12 AA LCDR3 lengths also increased (Fig. S3b).

Similar results were also observed with the donor YYQ. The percentage of IGHV3-53 and IGKV3-20, which encode  $V_H$  and  $V_K$  of 2YYQH9 increased from 1.99% to 2.73% and from 10.43% to 11.78% after immunization, respectively (Fig. 5b). For 2YYQF10 antibody, the percentage of IGHV1-2 that encode  $V_H$  rose from 3.53% to 5.12%, with IGKV2-28 encoding  $V_K$  decreased slightly from 5.36% to 4.47% after immunization (Fig. 5b). Furthermore, following an inactivated vaccine inoculation, the percentage repertoire of  $V_H$  with SHM rates below 5% increased, and the percentage repertoire of  $V_K$  with SHM rates below 4% or over 13% grew whereas the percentage repertoire of  $V_L$  with SHM rates less than 5% rose (Fig. S3a). Regarding the CDR3 length, we discovered that the percentage of sequences with over 13 AA HCDR3 increased, whereas the percentage of sequences with varying KCDR3 and LCDR3 lengths did not significantly differ. (Fig. S3b).

#### Phylogenetic analysis of antibodies SWA9, SWB8, SWC11, 2YYQH9 and 2YYQF10 from the antibody repertoire in two time points

To map the evolutionary route of broadly neutralizing antibodies, the identity-divergence two-dimensional (2D) plots were used to analyze the  $V_H/V_K$  repertoires of SWA9, SWB8, SWC11, 2YYQH9 and 2YYQF10 based on their separate germline-origin sequences in two time points, respectively. Unlike HIV neutralizing antibodies, these antibodies related to  $V_H/V_K$  sequences were barely detected in separate clusters in two time points in the 2D plots due to the low SHM rates (around 5%) (Fig. 6).

Next, we checked these neutralizing antibody-related sequences using a CDR3 identity method. The cut-off value for identifying sequences phylogenetically related to SWA9, SWB8, SWC11, 2YYQH9 or 2YYQF10 was an 85% HCDR3/KCDR3/LCDR3 amino acid identity to  $V_H/V_{K/L}$ . In donor SW, no SWA9-, SWB8- and SWC11-like  $V_H$  sequences were detected in the IGHV1-58, IGHV3-48 and IGHV3-53 germlines from both time points. However, 347 and 154 SWA9-like  $V_K$  sequences, 2,169 and 1,260 SWB8-related  $V_K$  sequences, and 86 and 443 SWC11-related  $V_K$  sequences were identified in the first and second time point, respectively (Fig. 6a, b, c). For donor YYQ, similarly, no 2YYQH9- or 2YYQF10-related  $V_H$  sequences and 2YYQH9-related  $V_K$  sequences were found in the YYQ antibody repertoire in two time points (Fig. 6d, e). Nevertheless, 7,075 and 7,383 2YYQF10-related  $V_K$  sequences were identified pre- and post-vaccine inoculation, respectively (Fig. 6e). These results indicate that  $V_H$  experiences greater selective pressure than  $V_K$  and emerges with a much lower frequency in the

antibody repertoire, which is in accordance with the fact that  $V_H$  principally binds with the RBD, as suggested by the structures of RBD-antibody complexes.

#### Discussion

In this research, we isolated a series of extremely potent monoclonal antibodies (mAbs) with high neutralizing potency against diverse pseudotype and live SARS-CoV-2 variants from three convalescents who recovered from a severe clinical syndrome of SARS-CoV-2 prototype virus infection. Among these isolated antibodies, six antibodies could bind RBD with high avidity and neutralized SARS-CoV-2 subvariants efficiently. We tested the in vivo effect in XBB.1.16 infected hamsters, which result was similar to other researches using Omicron sublineage-infected animal models [30–32]. Amid these six antibodies, 2YYQH9 and LQLD6HL cocktail could reduce the pathological features of hamsters' lungs caused by XBB.1.16, suggesting they are ideal mAb drug candidates for preventing and treating SARS-CoV-2 infection. Besides, we also resolved the antibody-RBD complex structures of three antibodies, studied the antibody repertoires of two convalescents, and explored the evolutionary path of five neutralizing antibodies.

The emergence of SARS-CoV-2 virus variants (particularly Omicron variants) raised global public health concerns for these variants had shown increased resistance to neutralizing antibodies and vaccines-immunized plasma [33, 34]. Xie's lab team had tested 247 human anti-RBD NAbS identified from SARS convalescents or SARS-CoV-2 vaccinees, showing that NAbS drugs including LY-CoV016/LY-CoV555 cocktail, REGN-CoV2 cocktail, AZD1061/AZD8895 cocktail, and BRII-196 were escaped by Omicron variants, while VIR7831 and DXP-604 still functioned, but at reduced efficacy [35]. Omicron strains such as BA.2.12.1, BA.4 and BA.5 even escape antibodies elicited by Omicron infection [36]. In this research, we found that prototype SARS-CoV-2 infection induced broadly neutralizing antibodies against Omicron VOCs. Specially, 2YYQH9 and LQLD6HL neutralized the Omicron variant XBB with  $IC_{50}$  values of 0.7  $\mu\text{g/mL}$  and 0.045  $\mu\text{g/mL}$  respectively. Also, these two antibodies could neutralize all the live virus of Omicron variants. Our results suggest that the prototype SARS-CoV-2 infection induces broadly neutralizing antibodies against the Omicron variant, which is in accordance with previous research [37].

The escape of Omicron variant to RBD-directed neutralizing antibodies has been widely studied. Cao et al. found that K417N, G446S, E484A and Q439R within RBD escaped the antibodies of class A-D (corresponds to class I-IV) despite these antibodies' epitopes overlap ACE2 binding motif [23]. Similar phenomena that

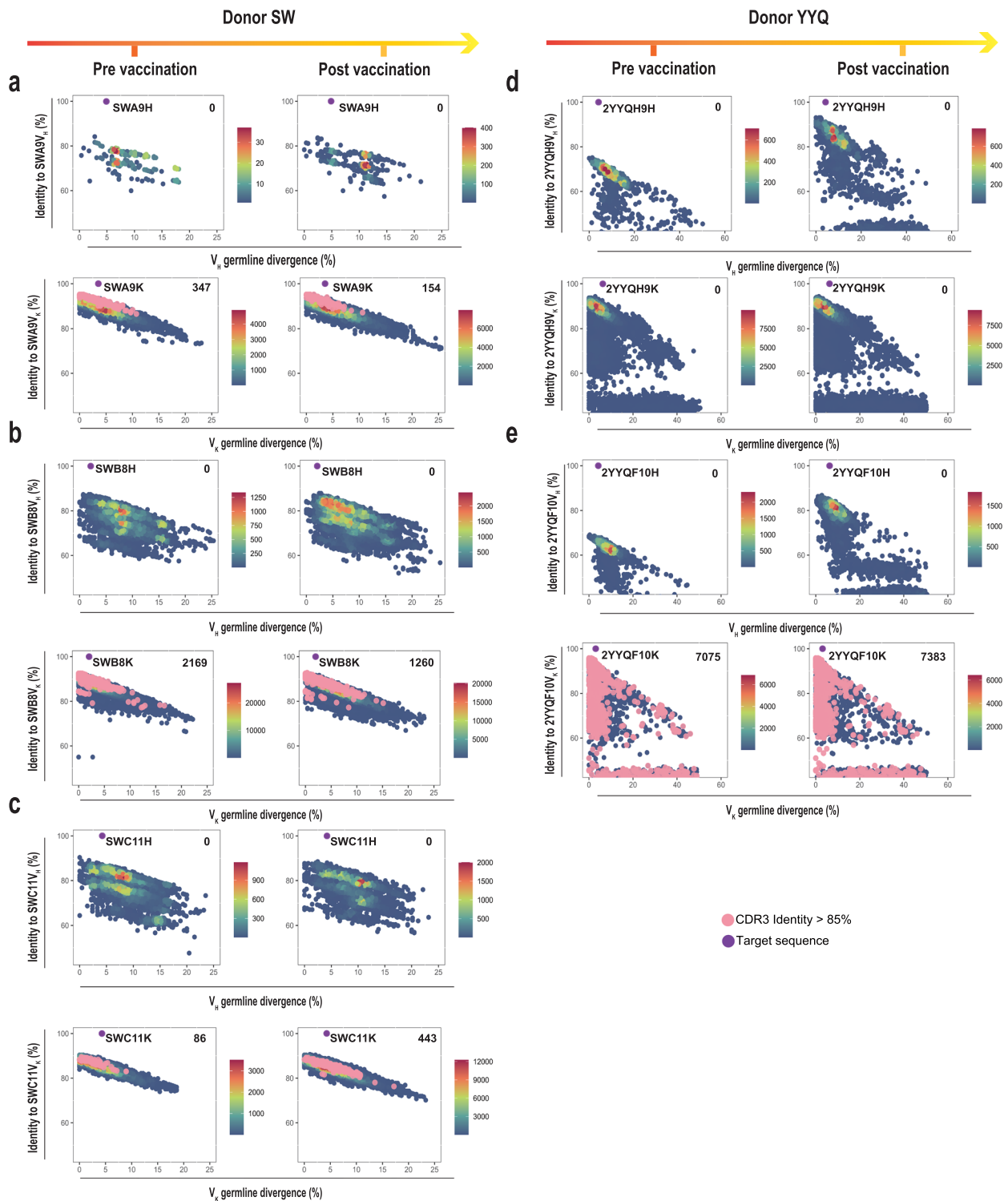


**Fig. 6** Identity-divergence analysis of the antibody amino acid sequences of SWA9, SWB8 and SWC11 of the donors in two time points (pre- and post- immunization). The x-axis and y-axis indicate the sequence diversities to the germline and the sequence identities to the antibody, respectively. Sequences presenting over 85% CDR3 identity with target antibody are colored pink. **(a)** SWA9 **(b)** SWB8 **(c)** SWC11 **(d)** 2YYQH9 **(e)** 2YYQF10

Omicron counteracts nAbs and vaccines were reported by Iketani et al. [38]. Planas et al. [39]. Cele et al. [40]. and Cameroni et al. [41]. Interestingly, we found that most of these antibodies were isolated from the samples which were collected shortly after infection (mainly less than 60 days). In contrast, the sample of donors SW, YYQ and LQL enrolled in this research was collected at 183 days after symptoms onset (Table S1). For SARS-CoV-2 RNA has been detected outside the lungs, including the brain, up to 230 days after symptom onset [42]. Thus, we postulate that potent neutralizing antibodies may keep evolving due to the stimulation of residual virus particles in human body.

We further characterized how two broadly neutralizing antibodies (SWA9 and SWC11) interact with the B.1.617.2 spike using cryo-EM. Our results show that SWA9 and SWC11 bind to the left shoulder and neck region of RBD and both directly block the interaction between RBD and ACE2. Most mutated sites found in the SARS-CoV-2 variants are not located in the epitopes of these two antibodies, rationalizing their potent activities towards the VOCs examined in this study. Interestingly, both SWA9 and SWC11 may contact Lys478 in the B.1.617.2 spike to gain additional interaction strength, which helps to explain their enhanced potency towards B.1.617.2. At the same time, we resolved the crystal structure of 2YYQH9/Omicron RBD and disclosed that the epitope of 2YYQH9 antibody nearly cover the whole RBM, indicating its potent and broad neutralizing activity. Recently, the combination of RBD-specific neutralizing antibodies SA55 and SA58 isolated from a SARS convalescent had been considered as potent candidates for preventing and treating SARS-CoV-2 infection [43]. However, BA.2.75, BA.2.75.2, BF.7, XBB, and BQ.1.1 escaped the neutralization of SA58 [7], indicating the efficient antibody cocktails should include novel potent neutralizing antibodies targeting diverse epitopes such as SWA9, SWC11 and 2YYQH9.

RBD-directed bNabs mostly originate from specific  $V_H$  germ lines such as IGHV1, IGHV3 and IGHV4 with relatively lower SHM rates (<10%) [10]. We also found that the majority of antibodies in this research presented those similar characteristics, indicating that RBD-specific Nabs arise from several  $V_H$  germ lines soon after infection, which is not consistent with HIV-1 CD4 binding site-directed antibodies such as VRC01-like antibodies which  $V_H$  mainly derive from IGHV1-2\*02 allele and have SHM rates over 15% [44]. Interestingly, we observed the increase of RBD-directed antibody-related germline frequencies and SHM rates after an inactivated vaccine immunization, which suggest that vaccination could help with RBD-directed Nabs evolution. Besides, although bNabs (SWA9, SWC11 and 2YYQH9) related antibodies

were barely detected in separate clusters in the 2D plots due to the low SHM rates (~5%), the CDR3 identity analysis clearly indicates that  $V_H$  receive greater selective pressure than  $V_K$ .

Our research has a limitation that only two antibodies, 2YYQH9 and LQLD6HL, were tested in a syrian hamster model prior to and post- SARS-CoV-2 infection to evaluate their in vivo functions. Since increasing Omicron variants emerge worldwide, the in vitro and in vivo study of these antibodies against newly predominant variants should be planned in the future.

## Conclusions

We identified six broadly neutralizing antibodies showing promise protective function against all the VOCs and some Omicron variants of SARS-CoV-2. The combination of these antibodies may offer a promising cocktail therapy to treat or prevent the future outbreaks of SARS-CoV-2 infection. The resolved antibody-antigen structure and deciphered antibodyome characteristics of special antibodies will contribute to the design of the vaccine and elite neutralizing antibody against newly emerging or re-emerging highly pathogenic SARS-CoV-2 variants.

## Supplementary Information

The online version contains supplementary material available at <https://doi.org/10.1186/s12967-025-06162-6>.

Supplementary material 1

## Author contributions

Dan Li, Caiqin Hu, Junwei Su, Shuo Du and Ying Zhang drafted the manuscript, initiated and coordinated the project. Zheng Wang, Junyu Xiao, and Yiming Shao designed the project. Wanqi Ni and Yanling Hao constructed the antibodies. Li Ren and Changzhong Jin evaluated the neutralizing potency. Yi Feng and Wanqi Ni analyzed the antibody sequence. Shuo Wang performed the cell sorting. Xinxian Dai performed the animal experiment. Biao Zhu provided the convalescent samples. All the authors have approved the manuscript.

## Funding

This research was supported by the National Natural Science Foundation of China (U20A20362, 92369103) and the State Key Laboratory of Infectious Disease Prevention and Control grant (2020SKLID102).

## Availability of data and materials

The datasets used and/or analyzed during the current study are available from the corresponding author on reasonable request.

## Declarations

### Ethics approval and consent to participate

The study was conducted in accordance with the Declaration of Helsinki, and approved by the Ethics Committee of the first affiliated hospital, Zhejiang University School of Medicine, China (approval number:2020-IIT-433). The patients/participants provided their written informed consent to participate in this study. Animal experiments were conducted according to the standard operating procedures approved by the National Vaccine & Serum institute

(NCSI) and complied with all relevant ethical regulations regarding animal research (Ethics Number: NCSI-RCD-JSDW-SER-2023031).

#### Consent for publication

All authors agreed to publish this study.

#### Competing interests

The authors declare that they have no competing interests.

#### Author details

<sup>1</sup>National Key Laboratory of Intelligent Tracking and Forecasting for Infectious Diseases, National Center for AIDS/STD Control and Prevention, Chinese Center for Disease Control and Prevention, Beijing 102206, China. <sup>2</sup>State Key Laboratory for Diagnosis and Treatment of Infectious Diseases, National Clinical Research Center for Infectious Diseases, Collaborative Innovation Center for Diagnosis and Treatment of Infectious Diseases, The First Affiliated Hospital, School of Medicine, Zhejiang University, Hangzhou 310003, China. <sup>3</sup>Changping Laboratory, Beijing 102206, China. <sup>4</sup>State Key Laboratory of Protein and Plant Gene Research, School of Life Sciences, Peking University, Beijing 100091, China. <sup>5</sup>National Vaccine and Serum Institute, Beijing 101111, China. <sup>6</sup>China National Biotec Group Company Limited, Beijing 100024, China. <sup>7</sup>Peking-Tsinghua Center for Life Sciences, Peking University, Beijing 100091, China.

Received: 13 September 2024 Accepted: 22 January 2025

Published online: 21 February 2025

#### References

- Piekos SN, Price ND, Hood L, Hadlock JJ. The impact of maternal SARS-CoV-2 infection and COVID-19 vaccination on maternal-fetal outcomes. *Reprod Toxicol*. 2022;114:33–43.
- Ntounis T, Prokopakis I, Koutras A, Fasoulakis Z, Pittokopitou S, Valsamaki A, Chionis A, Kontogeorgi E, Lampraki V, Peraki A, et al. Pregnancy and COVID-19. *J Clin Med*. 2022. <https://doi.org/10.3390/jcm11226645>.
- Richardson SJ, Madzorer A, Spencer H, Manamela NP, van der Mescht MA, Lambson BE, Oosthuysen B, Ayres F, Makhado Z, Moyo-Gwete T, et al. SARS-CoV-2 Omicron triggers cross-reactive neutralization and Fc effector functions in previously vaccinated, but not unvaccinated, individuals. *Cell Host Microbe*. 2022;30:880–6.
- Adeniji OS, Giron LB, Purwar M, Zilberstein NF, Kulkarni AJ, Shaikh MW, Balk RA, Moy JN, Forsyth CB, Liu Q, et al. COVID-19 Severity Is Associated with Differential Antibody Fc-Mediated Innate Immune Functions. *mBio*. 2021. <https://doi.org/10.1128/mBio.01244-21>.
- Yang L, Liu W, Yu X, Wu M, Reichert JM, Ho M. COVID-19 antibody therapeutics tracker: a global online database of antibody therapeutics for the prevention and treatment of COVID-19. *Antib Ther*. 2020;3:205–12.
- Baral PK, Yin J, James M. Treatment and prevention strategies for the COVID 19 pandemic: a review of immunotherapeutic approaches for neutralizing SARS-CoV-2. *Int J Biol Macromol*. 2021;186:490–500.
- Cao Y, Jian F, Wang J, Yu Y, Song W, Yisimayi A, Wang J, An R, Chen X, Zhang N, et al. Imprinted SARS-CoV-2 humoral immunity induces convergent Omicron RBD evolution. *Nature*. 2023;614:521–9.
- Jeworowski LM, Muhlemann B, Walper F, Schmidt ML, Jansen J, Krumbholz A, Simon-Loriere E, Jones TC, Corman VM, Drosten C. Humoral immune escape by current SARS-CoV-2 variants BA.2.86 and JN.1, December 2023. *Euro Surveill*. 2024. <https://doi.org/10.2807/1560-7917.ES.2024.29.2.2300740>.
- Planas D, Staropoli I, Michel V, Lemoine F, Donati F, Prot M, Porrot F, Guivel-Benhassine F, Jeyarajah B, Brisebarre A, et al. Distinct evolution of SARS-CoV-2 Omicron XBB and BA.2.86 lineages combining increased fitness and antibody evasion. *Nature Communication*. 2024;15:2254.
- Chen Y, Zhao X, Zhou H, Zhu H, Jiang S, Wang P. Broadly neutralizing antibodies to SARS-CoV-2 and other human coronaviruses. *Nat Rev Immunol*. 2023;23:189–99.
- Barnes CO, Jette CA, Abernathy ME, Dam KA, Esswein SR, Gristick HB, Maljutin AG, Sharaf NG, Huey-Tubman KE, Lee YE, et al. SARS-CoV-2 neutralizing antibody structures inform therapeutic strategies. *Nature*. 2020;588:682–7.
- Shi R, Shan C, Duan X, Chen Z, Liu P, Song J, Song T, Bi X, Han C, Wu L, et al. A human neutralizing antibody targets the receptor-binding site of SARS-CoV-2. *Nature*. 2020;584:120–4.
- Kim C, Ryu DK, Lee J, Kim YI, Seo JM, Kim YG, Jeong JH, Kim M, Kim JI, Kim P, et al. A therapeutic neutralizing antibody targeting receptor binding domain of SARS-CoV-2 spike protein. *Nat Commun*. 2021;12:288.
- Jones BE, Brown-Augsburger PL, Corbett KS, Westendorf K, Davies J, Cujec TP, Wiethoff CM, Blackbourne JL, Heinz BA, Foster D, et al. The neutralizing antibody, LY-CoV555, protects against SARS-CoV-2 infection in nonhuman primates. *Sci Transl Med*. 2021. <https://doi.org/10.1126/scitranslmed.abf1906>.
- Luo S, Zhang J, Kreutzberger A, Eaton A, Edwards RJ, Jing C, Dai HQ, Sempowski GD, Cronin K, Parks R, et al. An antibody from single human V(H)-rearranging mouse neutralizes all SARS-CoV-2 variants through BA5 by inhibiting membrane fusion. *Sci Immunol*. 2022;7:eadd5446.
- Zhou T, Wang L, Misasi J, Pegu A, Zhang Y, Harris DR, Olin AS, Talana CA, Yang ES, Chen M, et al. Structural basis for potent antibody neutralization of SARS-CoV-2 variants including B.1.1.529. *Science*. 2022;376:eabn8897.
- Yuan M, Wu NC, Zhu X, Lee CD, So R, Lv H, Mok C, Wilson IA. A highly conserved cryptic epitope in the receptor binding domains of SARS-CoV-2 and SARS-CoV. *Science*. 2020;368:630–3.
- Wang Z, Li D, Chen Y, Sun Y, Jin C, Hu C, Feng Y, Su J, Ren L, Hao Y, et al. Characterization of RBD-specific cross-neutralizing antibodies responses against SARS-CoV-2 variants from COVID-19 convalescents. *Front Immunol*. 2023;14:1160283.
- Nie J, Li Q, Wu J, Zhao C, Hao H, Liu H, Zhang L, Nie L, Qin H, Wang M, et al. Quantification of SARS-CoV-2 neutralizing antibody by a pseudo-typed virus-based assay. *Nat Protoc*. 2020;15:3699–715.
- Hu Y, Li D, Yuan Z, Feng Y, Ren L, Hao Y, Wang S, Hu X, Liu Y, Hong K, et al. Characterization of a VRC01-like antibody lineage with immature VL from an HIV-1 infected Chinese donor. *Mol Immunol*. 2023;154:11–23.
- Du S, Cao Y, Zhu Q, Yu P, Qi F, Wang G, Du X, Bao L, Deng W, Zhu H, et al. Structurally resolved SARS-CoV-2 antibody shows high efficacy in severely infected hamsters and provides a potent cocktail pairing strategy. *Cell*. 2020;183:1013–23.
- Punjani A, Rubinstein JL, Fleet DJ, Brubaker MA. cryoSPARC: algorithms for rapid unsupervised cryo-EM structure determination. *Nat Methods*. 2017;14:290–6.
- Du S, Liu P, Zhang Z, Xiao T, Yasimayi A, Huang W, Wang Y, Cao Y, Xie XS, Xiao J. Structures of SARS-CoV-2 B.1.351 neutralizing antibodies provide insights into cocktail design against concerning variants. *Cell Res*. 2021;31:1130–3.
- Emsley P, Lohkamp B, Scott WG, Cowtan K. Features and development of Coot. *Acta Crystallogr D Biol Crystallogr*. 2010;66:486–501.
- Petterson EF, Goddard TD, Huang CC, Meng EC, Couch GS, Croll TI, Morris JH, Ferrin TE. UCSF ChimeraX: Structure visualization for researchers, educators, and developers. *Protein Sci*. 2021;30:70–82.
- Ju B, Zhang Q, Ge J, Wang R, Sun J, Ge X, Yu J, Shan S, Zhou B, Song S, et al. Human neutralizing antibodies elicited by SARS-CoV-2 infection. *Nature*. 2020;584:115–9.
- Cao Y, Su B, Guo X, Sun W, Deng Y, Bao L, Zhu Q, Zhang X, Zheng Y, Geng C, et al. Potent neutralizing antibodies against SARS-CoV-2 identified by high-throughput single-cell sequencing of convalescent patients' B cells. *Cell*. 2020;182:73–84.
- Dejnirattisai W, Zhou D, Ginn HM, Duyvesteyn H, Supasa P, Case JB, Zhao Y, Walter TS, Mentzer AJ, Liu C, et al. The antigenic anatomy of SARS-CoV-2 receptor binding domain. *Cell*. 2021;184:2183–200.
- Dejnirattisai W, Huo J, Zhou D, Zahradnik J, Supasa P, Liu C, Duyvesteyn H, Ginn HM, Mentzer AJ, Tuekprakhon A, et al. SARS-CoV-2 Omicron-B.1.1.529 leads to widespread escape from neutralizing antibody responses. *Cell*. 2022;185:467–84.
- Tamura T, Ito J, Uriu K, Zahradnik J, Kida I, Anraku Y, Nasser H, Shofa M, Oda Y, Lytras S, et al. Virological characteristics of the SARS-CoV-2 XBB variant derived from recombination of two Omicron subvariants. *Nat Commun*. 2023;14:2800.
- Mohandas S, Shete A, Kumar A, Wakchaure K, Rai V, Mote C, Dighe H, Sarkale P, Gawande P, Yemul J, et al. Comparative pathogenicity of BA.2.12, BA.5.2 and XBB.1 with the delta variant in Syrian hamsters. *Front Microbiol*. 2023;14:1183763.

32. Halfmann PJ, Iwatsuki-Horimoto K, Kuroda M, Hirata Y, Yamayoshi S, Iida S, Uraki R, Ito M, Ueki H, Furusawa Y, et al. Characterization of Omicron BA.4.6, XBB, and BQ.1.1 subvariants in hamsters. *Commun Biol.* 2024;7:331.
33. Carabelli AM, Peacock TP, Thorne LG, Harvey WT, Hughes J, Peacock SJ, Barclay WS, de Silva TI, Towers GJ, Robertson DL. SARS-CoV-2 variant biology: immune escape, transmission and fitness. *Nat Rev Microbiol.* 2023;21:162–77.
34. Harvey WT, Carabelli AM, Jackson B, Gupta RK, Thomson EC, Harrison EM, Ludden C, Reeve R, Rambaut A, Peacock SJ, Robertson DL. SARS-CoV-2 variants, spike mutations and immune escape. *Nat Rev Microbiol.* 2021;19:409–24.
35. Cao Y, Wang J, Jian F, Xiao T, Song W, Yisimayi A, Huang W, Li Q, Wang P, An R, et al. Omicron escapes the majority of existing SARS-CoV-2 neutralizing antibodies. *Nature.* 2022;602:657–63.
36. Cao Y, Yisimayi A, Jian F, Song W, Xiao T, Wang L, Du S, Wang J, Li Q, Chen X, et al. BA.2.12.1, BA.4 and BA.5 escape antibodies elicited by Omicron infection. *Nature.* 2022;608:593–602.
37. Ju B, Zhang Q, Wang Z, Aw ZQ, Chen P, Zhou B, Wang R, Ge X, Lv Q, Cheng L, et al. Infection with wild-type SARS-CoV-2 elicits broadly neutralizing and protective antibodies against omicron subvariants. *Nat Immunol.* 2023;24:690–9.
38. Iketani S, Liu L, Guo Y, Liu L, Chan JF, Huang Y, Wang M, Luo Y, Yu J, Chu H, et al. Antibody evasion properties of SARS-CoV-2 Omicron sublineages. *Nature.* 2022;604:553–6.
39. Planas D, Saunders N, Maes P, Guivel-Benhassine F, Planchais C, Buchrieser J, Bolland WH, Porrot F, Staropoli I, Lemoine F, et al. Considerable escape of SARS-CoV-2 Omicron to antibody neutralization. *Nature.* 2022;602:671–5.
40. Cele S, Jackson L, Khoury DS, Khan K, Moyo-Gwete T, Tegally H, San JE, Cromer D, Scheepers C, Amoako DG, et al. Omicron extensively but incompletely escapes Pfizer BNT162b2 neutralization. *Nature.* 2022;602:654–6.
41. Cameron E, Bowen JE, Rosen LE, Saliba C, Zepeda SK, Culap K, Pinto D, VanBlargan LA, De Marco A, di Iulio J, et al. Broadly neutralizing antibodies overcome SARS-CoV-2 Omicron antigenic shift. *Nature.* 2022;602:664–70.
42. Stein SR, Ramelli SC, Grazioli A, Chung JY, Singh M, Yinda CK, Winkler CW, Sun J, Dickey JM, Ylaya K, et al. SARS-CoV-2 infection and persistence in the human body and brain at autopsy. *Nature.* 2022;612:758–63.
43. Cao Y, Jian F, Zhang Z, Yisimayi A, Hao X, Bao L, Yuan F, Yu Y, Du S, Wang J, et al. Rational identification of potent and broad sarbecovirus-neutralizing antibody cocktails from SARS convalescents. *Cell Rep.* 2022;41:111845.
44. Zhou T, Zhu J, Wu X, Moquin S, Zhang B, Acharya P, Georgiev IS, Altae-Tran HR, Chuang GY, Joyce MG, et al. Multidonor analysis reveals structural elements, genetic determinants, and maturation pathway for HIV-1 neutralization by VRC01-class antibodies. *Immunity.* 2013;39:245–58.

## Publisher's Note

Springer Nature remains neutral with regard to jurisdictional claims in published maps and institutional affiliations.